

Improvement the formaldehyde sensing and detection through Pt-doped graphdiyne monolayer: Quantum chemical study

Mohamed J. Saadh^a, Hala Kh. Mohammed^b, A.J. Ameer^c, Shelesh Krishna Saraswat^{d,*},
Sura Mohammad Mohealdeen^e, H.A. AL Sailaw^f, Mustafa Mudhafar^g, Farah A. Dawood^h,
 Yasser Elmasryⁱ

^a Faculty of Pharmacy, Middle East University, Amman 11831, Jordan

^b Medical Laboratory Techniques Department, Almaarif University College, Ramadi, Iraq

^c Al-Zahraa University for Women, Karbala, Iraq

^d Department of Electronics and Communication Engineering, GLA University, Mathura-281406, India

^e Department of Radiology & Sonar Techniques, Al-Noor University College, Nineveh, Iraq

^f Department of Chemistry and Biochemistry, Faculty of Medicine, University of Kerbala, 56001, Karbala, Iraq

^g Department of Medical Physics, College of Applied Medical Sciences, University of Kerbala, 56001 Karbala, Iraq

^h Department of Medical Laboratories Technology, AL-Nisour University College, Baghdad, Iraq

ⁱ Department of Mathematics, Faculty of Science, King Khalid University, P.O. Box 9004, Abha 61466, Saudi Arabia

ARTICLE INFO

Keywords:

Formaldehyde
 Graphdiyne
 Electrostatic potentials
 Gas sensors

ABSTRACT

One of the commonly employed chemical feedstocks is formaldehyde (CH₂O), which has diverse applications in many fields. However, CH₂O might have detrimental effects on human because of its toxicity. Hence, it is of utmost significance to effectively monitor and detect CH₂O. Within this piece of research, the adhesion attributes of the pristine graphdiyne (PGRD) and Pt-doped GRD (Pt@GRD) for CH₂O were examined through DFT calculations. Moreover, the HOMO-LUMO energy levels, electrostatic potentials, energy band structures, adhesion structure parameters, and doping site optimizations of the Pt@GRD were investigated. Based on the results, doping the Pt atom the optimal site (CII) dramatically reduced the energy gap and substantially enhanced the electrical conductance. The PGRD was not suitable for the detection of CH₂O with high sensitivity since it used mainly physisorption. However, there was a robust chemical adsorption between Pt@GRD and CH₂O via the chemical reaction and hybridization of the Pt-d orbital with the molecular orbital of CH₂O. The performance of Pt@GRD as a novel 2D material in detecting CH₂O was extremely high. The current results can provide useful insights into developing future sensors for the detection of various gasses.

1. Introduction

In recent years, the emission of hazardous pollutants from soil, air and water has been one the undesirable outcomes of industrial developments, which has negatively impacted on the human health as well as the on climate. Formaldehyde (CH₂O) is one these pollutants, which has a pungent smell and it is colorless [1]. In different chemical industries such as house detergents, cosmetics, food preservation, paints, adhesives and textile industry, CH₂O is used as an important reagent [2–5]. Moreover, CH₂O is liberated from furniture [9] and it can be generated from a photochemical reaction [6,7]. There are common side effects associated with CH₂O as a toxic material [8], for example nasal

tumors, nasopharyngeal cancer, harm to the endocrine and nervous systems and inflammation of the eyes [9–11]. Considering the above-mentioned facts, finding a suitable material capable of removing CH₂O or being used as a CH₂O sensors is of utmost significance.

Owing to their simple fabrication method, cost-effectiveness and high sensitivity to diverse gasses, semiconducting gas sensors based on metal oxides have been replaced with old technologies such as gas chromatography and mass spectrometry, which is turn due to the developments made in nanotechnology [12–14]. Nevertheless, there are several drawbacks to metal oxide-based gas sensors like long recovery-response and high operating temperatures [15]. The above-mentioned drawbacks were overcome after the advent of 2D materials [16]

* Corresponding author.

E-mail address: sheleshkrishnasaraswat@gmail.com (S.K. Saraswat).

<https://doi.org/10.1016/j.diamond.2023.110560>

Received 7 August 2023; Received in revised form 20 October 2023; Accepted 29 October 2023

Available online 31 October 2023

0925-9635/© 2023 Elsevier B.V. All rights reserved.

thanks to their unique attributes such high surface sensitivity to the environment, superior optical properties, high surface activity, chemical inertness and high specific surface area. These attributes have made 2D materials ideal for different applications in the chemical sensing field [17–21]. As an instance, one of sensing materials used for the detection of NO was MoS₂ [22]. Moreover, graphene (Gr) was demonstrated to be capable of sensing carbon dioxide, and the monolayer graphene had a noticeable impact upon the adhesion strength and the charge transport of NO molecules [23–27].

One of the newly discovered members of 2D carbon-based nano-materials is graphdiyne (GRD), which is a diacetyl carbon isotope with most stability [28–30]. In comparison to Gr, GRD has unique attributes such as high physical stability and chemical activity because of its unique C atom structure with sp- and sp² hybridization [31–36]. Such unique properties are not only conducive to the transport of electrons, but also provide it with great performance in catalysis and adhesion [37]. GRD has the potential to be used for different purposes such as gas separation, sensing, catalysis and energy storage. In a study by Kim and Lee et al., GRD demonstrated a dramatic increase in the adhesion of SO₂ after it was doped by nitrogen and after a single C atom defect was introduced [38]. In a study by Lu et al., the Mn-doped GRD sensing response towards different gasses like NH₃ and CO was investigated [39]. In a study by Zhang et al., Pd-doped GR was used for monitoring dissolved gasses in the transformer oil [40]. In another study by Hussain et al., nitride pore GRD, GRD as well as its heterogeneous structure were used for analyzing the gas sensitiveness of volatile organic compounds [41]. In a study by Zhao et al., the introduction of sp-N dopant was demonstrated to be conducive to the adhesion and electron transport of oxygen in GRD [42]. The above-mentioned pieces of research not only demonstrate the suitability of GRD as a gas sensor, but also show that its modification through doping can enhance its attributes. Doping C-based materials through metal and non-metal atoms can increase their electrical conductance and their thermal stability. Also, it can increase their mechanical response properties and optical index [43]. Platinum (Pt) is a well-known and commonly used catalyst in various fields because of its high catalytic activity and stability. Therefore, Pt doping could enhance the catalytic performance of graphene-based materials. The Pt atoms have unique electronic, structural, and surface properties that make them suitable for enhancing chemical reactions. In addition, Pt atoms have a high surface area, which can improve the efficiency of charge transfer and enhance electrocatalytic performance. Furthermore, Pt atom doping can lead to changes in the electronic structure of the graphene-like materials, which can result in improved energy level alignment. Hence, it was assumed that doping GRD with the Pt atom could increase its adhesion performance as a gas sensor [44]. Nonetheless, few research studies have investigated the adhesion attributes of GRD and its modified materials for CH₂O.

Within this piece of research, atomic simulations were carried out to investigate the structural attributes of Pt-doped GRD (Pt@GRD). A GRD surface model and the Pt@GRD were optimized and developed using the first-principles DFT. Several properties of CH₂O such as the HOMO/LUMO energy level difference, electrostatic potential, density of states and adhesion energy, were investigated to understand its intrinsic adhesion mechanism on the surface of pristine GRD (PGRD) and Pt@GRD. The results can provide insights into the application of GRD as a gas sensing material, as well as modification and use of 2D C-based materials.

2. Computational details

The GAMESS software was applied for performing the calculations in this work [45]. The B3LYP/6-31G* method was adopted in order to perform NBO, electronic-energy analyses and structural optimizations. For the sake of evaluating London and Van der Waals forces accurately, we included the term “D3” [46]. According to the literature, B3LYP, which has widespread applications, is incapable of calculating

dispersion interactions [47–50]. After the full structural optimizations, the harmonics were also computed to demonstrate that structures with a positive frequency are true local minima. The binding energy (BE) was computed as below to evaluate the stability of Pt@GRD:

$$E_a = E_{Pt-GDY} - E_{GDY} - E_{Pt} \quad (1)$$

where the energies of a single Pt atom, the PGRD and that of the system after doping are designated by E_{Pt} , E_{GDY} and E_{Pt-GDY} [51]. The adhesion energy of EGDY on the surface of PGRD and Pt@GRD was calculated as follows:

$$E_{ad} = E_{Pt-GDY/gas} - E_{Pt-GDY} - E_{gas} \quad (2)$$

where the total energy of a single CH₂O molecule, the energy of the Pt@GRD prior to the adhesion of CH₂O, and the energy of Pt@GRD following the adhesion of CH₂O are designated by E_{Gas} , E_{Pt-GDY} and $E_{Pt-GDY/gas}$, [52]. The adhesion performance of substrate materials on adsorbents can be assessed using the adhesion energy. The negative value of adhesion energy demonstrates the spontaneous adhesion of gas molecules the absolute adhesion energy value demonstrates the stability of the adhesion process [53]. The energy values of HOMO and LUMO are used to represent electron affinity (A) and ionization energy (I), respectively. Specifically, IE is equivalent to the negative value of HOMO, while EA is equivalent to the negative value of LUMO. The stability and structural reactivity of a material can be determined by utilizing its global chemical potential (μ), electronegativity (χ), hardness (η), and electrophilicity index (ω). These properties can be calculated through the following equations [54]:

$$\mu = -(I + A)/2 \quad (3)$$

$$\chi = (I + A)/2 \quad (4)$$

$$\eta = (I - A)/2 \quad (5)$$

$$\omega = \mu^2/2\eta \quad (6)$$

The following equation can calculate the amount of energy of solvation (E_{solv}) which is used to determine the complexes' solubility in the solvent phase [55]:

$$E_{solv} = E_{sol} - E_{gas} \quad (7)$$

where, E_{sol} , and E_{gas} denote the complex's net energy in the solvent and gas phase, respectively. A polarized continuum model (PCM) was used to determine the effects of solvent (H₂O) [56].

3. Results and discussion

3.1. Structural optimizations of PGRD and Pt@GRD

We established the GRD crystal structure with a lattice parameter of $a = b = 19.15 \text{ \AA}$, $\alpha = \beta = 90^\circ$ and $\gamma = 120^\circ$. As depicted in Fig. 1, after the geometric structure was optimized, 4 different C–C bond types of GRD (Csp²-Csp², Csp²-Csp, Csp-Csp', Csp'-Csp') had a length of 1.45 Å, 1.42 Å, 1.24 Å, 1.36 Å respectively [57]. Three doping sites could be replaced according to the different hybridization types of C atoms in GRD, namely CI, CII, and CIII. Fig. 2 shows their structures [58]. As shown in Table 1, based on the energy computations, CII had the lowest BE, so it was selected as the best site for doping the Pt atom. After doping the Pt atom, the Pt atom was replaced with the C atom in the optimized structure of GRD at site CII. As shown in Fig. 3, after doping the Pt atom, there was no noticeable deformation in the structure of Pt@GRD and it changed slightly. For example, the length of Pt-CI bond changed from 1.42 Å to 1.96 Å in comparison with the initial CI-CII bond and Pt-CIII bond length changed from 1.24 Å to 1.87 Å in comparison with the initial CII-CIII bond, which was due to the fact that the Pt atom had larger atomic radius than the C atom and its electronegativity was different, thereby

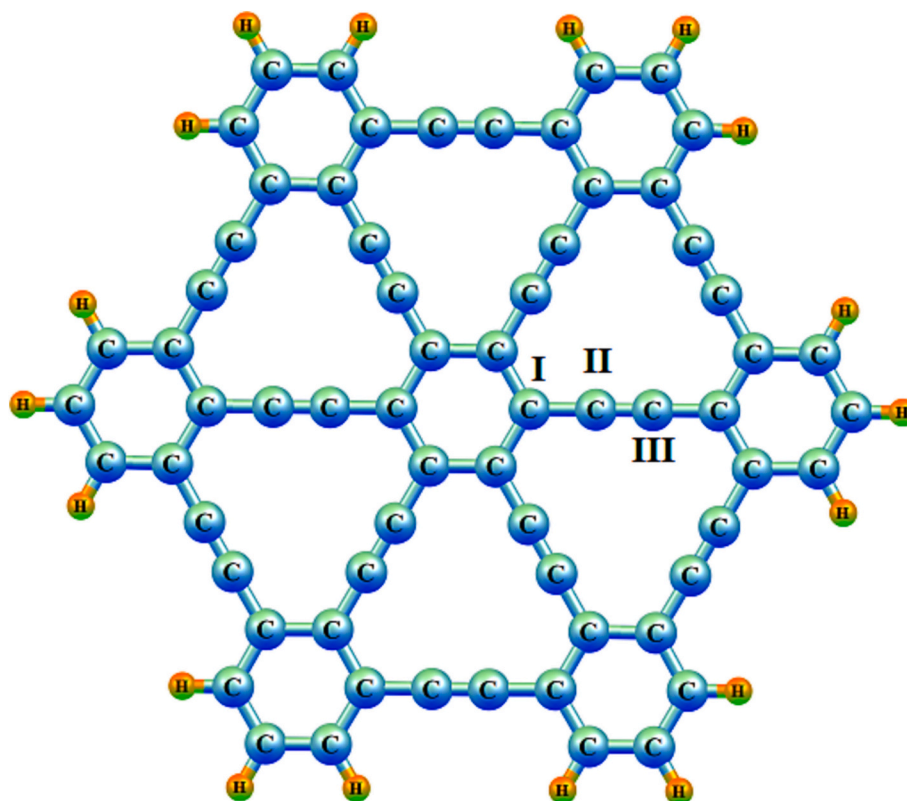


Fig. 1. The optimized geometry of GRD.

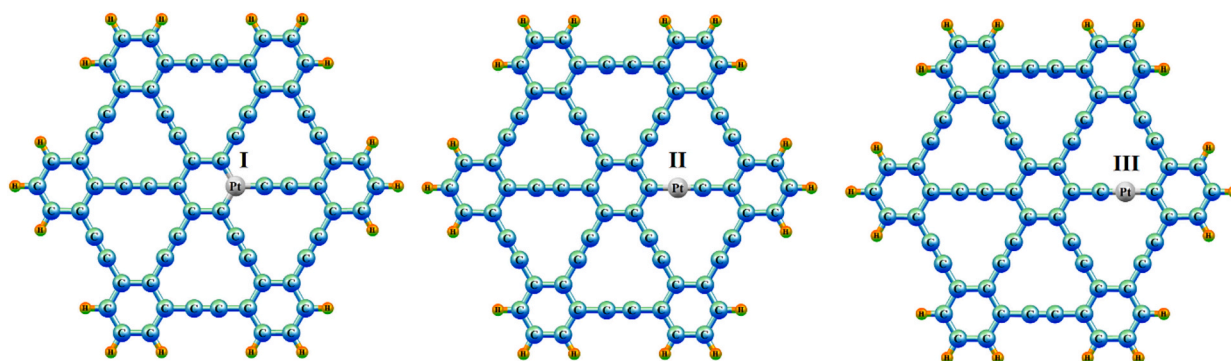


Fig. 2. Schematic plot of the structure of the three doping regions.

Table 1

Binding energies (E_a), bond lengths (D), and bandgap (E_g) of various doping regions in GRD.

Doping site	E_a (eV)	D (Å)	E_g (eV)
I	-4.217	1.96	2.32
II	-7.046	1.87	1.95
III	-5.128	1.92	2.18

causing a negligible alteration in the structure of Pt@-GRD. This alteration provided an empty space for the adhesion of CH_2O molecules [59]. The charge distribution of PGRD and Pt@GRD were obtained by performing the Mulliken population analysis. In the PGRD, sp^2 hybridized C atoms had a negative charge, whereas the sp hybridized one had a positive charge. Pt@GRD underwent noticeable charge transport, which indicated the impact of doping the Pt atom on changing the electronic reactivity of PGRD.

Fig. 4 demonstrates the DOS and the electronic band structures of PGRD and Pt@GRD. By comparing the energy bands, we can see the bandgap of PGRD was 2.46 eV, whereas that of the Pt@GRD decreased to 1.95 eV the Pt atom was doped. This shows that doping the Pt atom facilitated the transmission of electrons on the surface of doped GRD, which allowed an easy jumping from the valence band (VB) to the conduction band (CB) and thus leading to a rise in conductance. There was perfect symmetry in the DOS diagrams of the spin-down and self-selected rising images of PGRD and Pt@GRD, which confirmed that they were not magnetic and that there was a noticeable rise in the DOS at the Fermi level energy, which reconfirms that doping the Pt atom is capable of increasing the conductance of GRD, showing that there is a robust orbital interaction between the surface of GRD and the Pt atoms. This shows the stability of Pt@GRD-doped GDY and the fact that it improves the conductance of GRD, which lead to superior attributes for the adhesion of gas molecules.

The study investigated the interaction of CH_2O with Pt@GRD in the

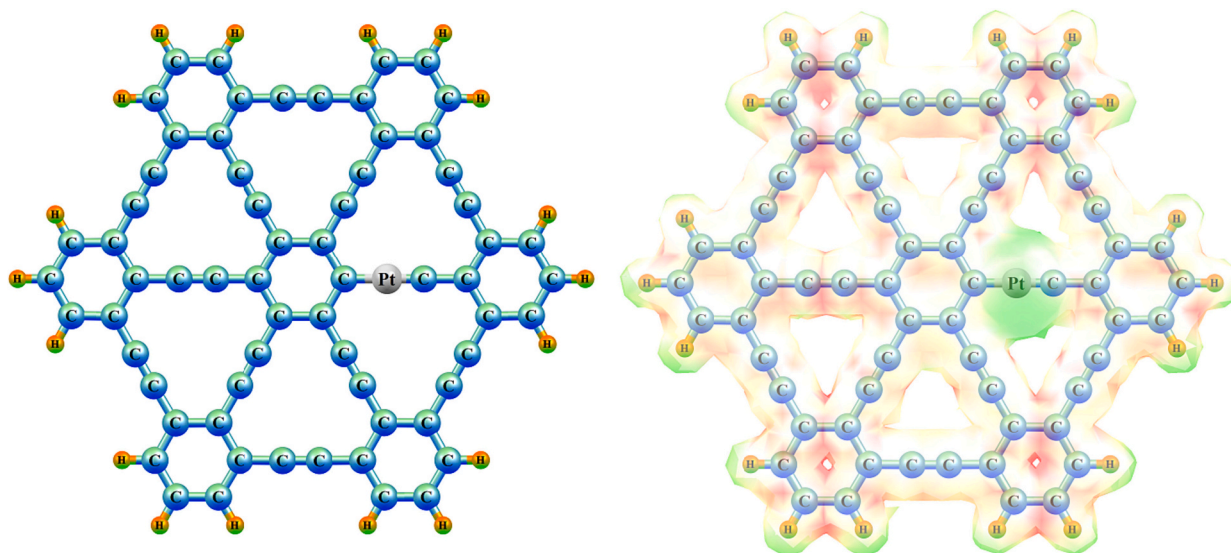


Fig. 3. The optimized geometry of the GRD following the Pt atom doping.

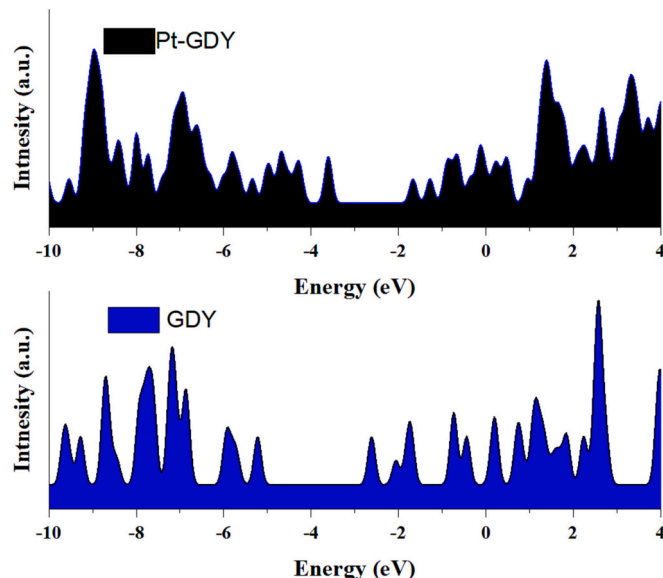


Fig. 4. The density of states plots of (a) GRD and (b) Pt@GRD.

presence of solvents. The difference between the calculated E_{ad} in gas and solution phases indicated stronger interactions in the solution phase, with more negative E_{ad} values confirming this. The E_{ad} of CH_2O in the gas phase was -1.57 kcal/mol, which increased to -2.32 kcal/mol in a water medium. This suggests that in a solvent medium, the solubility of CH_2O molecules increases, leading to an increased value of adsorption energy.

3.2. The adhesion of CH_2O onto PGRD

The adhesion parameters and configurations (CFGs) related to the

Table 2

Adhesion energies (E_{ads}), adhesion distance (D), and bandgap (E_g) of the CH_2O adhered onto the PGRD.

Systems	E_{ads} (eV)	D (\AA)	E_g (eV)
GRD	–	–	2.46
GRD- CH_2O	-0.417	2.04	2.39

adhesion of CH_2O by GRD are demonstrated in Table 2 and Fig. 5, which were computed using rational structural optimization and computations. Based on the findings, the adhesion of CH_2O molecules did not deform the geometry of GRD significantly and CH_2O molecules remained mainly in their initial structure. Moreover, as shown in Table 2, the absolute adhesion energy value was less than 0.5 eV for the CH_2O adsorbed system [60], which indicated the amount of energy exchange between CH_2O and GRD was negligible and the adhesion nature was physical. Based on the results, CH_2O had a physical adhesion on the PGRD. Despite the interaction between atomic orbitals, it was not strong enough, so the PGRD can be used a suitable sensing material to monitor gases. Hence, improving the adhesion attributes by doping the Pt atom is necessary.

3.3. The adhesion of CH_2O onto Pt@GRD

Based on previously performed structural optimizations and BE computations, Pt doping at site CII had the highest stability. To compare the performance of Pt@GRD and PGRD in adsorbing CH_2O , the adhesion site above the Pt atom was selected as the only initial adhesion site. Fig. 6 shows the final adhesion CFG after the structure was optimized. Following the full relaxation, the Pt@GRD whose atoms were in the same plane bend noticeably following the adhesion of CH_2O at the Pt-doped side. Moreover, there was a considerable change in the energetic and structural parameters following the adhesion of CH_2O (see Table). As an instance, the Pt–C1 bond increased from 1.93 \AA to 2.08 \AA following the adhesion of CH_2O . The structural changes indicated that there were robust interactions between the surface of Pt@GRD and CH_2O . As shown in Table 3, the absolute adhesion energy values for Pt@GRD for CH_2O was more than 1.57 eV. This indicated the chemical adsorption of CH_2O on the Pt@GRD.

The energy band structures for the adhesion of CH_2O were analyzed computationally for carefully investigating the relationship between the adsorption mechanism and the electronic attributes. As shown in Table 3, the bandgap of the original Pt@GRD was 1.95 eV, whereas the bandgap after the adhesion of CH_2O decreased noticeably to 1.19 eV, which demonstrates a noticeable change prior to the adhesion. The decreased distance between the VB and the CB resulted in an easier electron excitation for electron jumping, thereby enhancing the conductance of the system. This demonstrated that CH_2O adhesion attributes of modified GRD after doping the Pt atom were better. A comparison of the earlier energy band structure analysis, doping the Pt atom noticeably increased the adhesion performance of CH_2O .

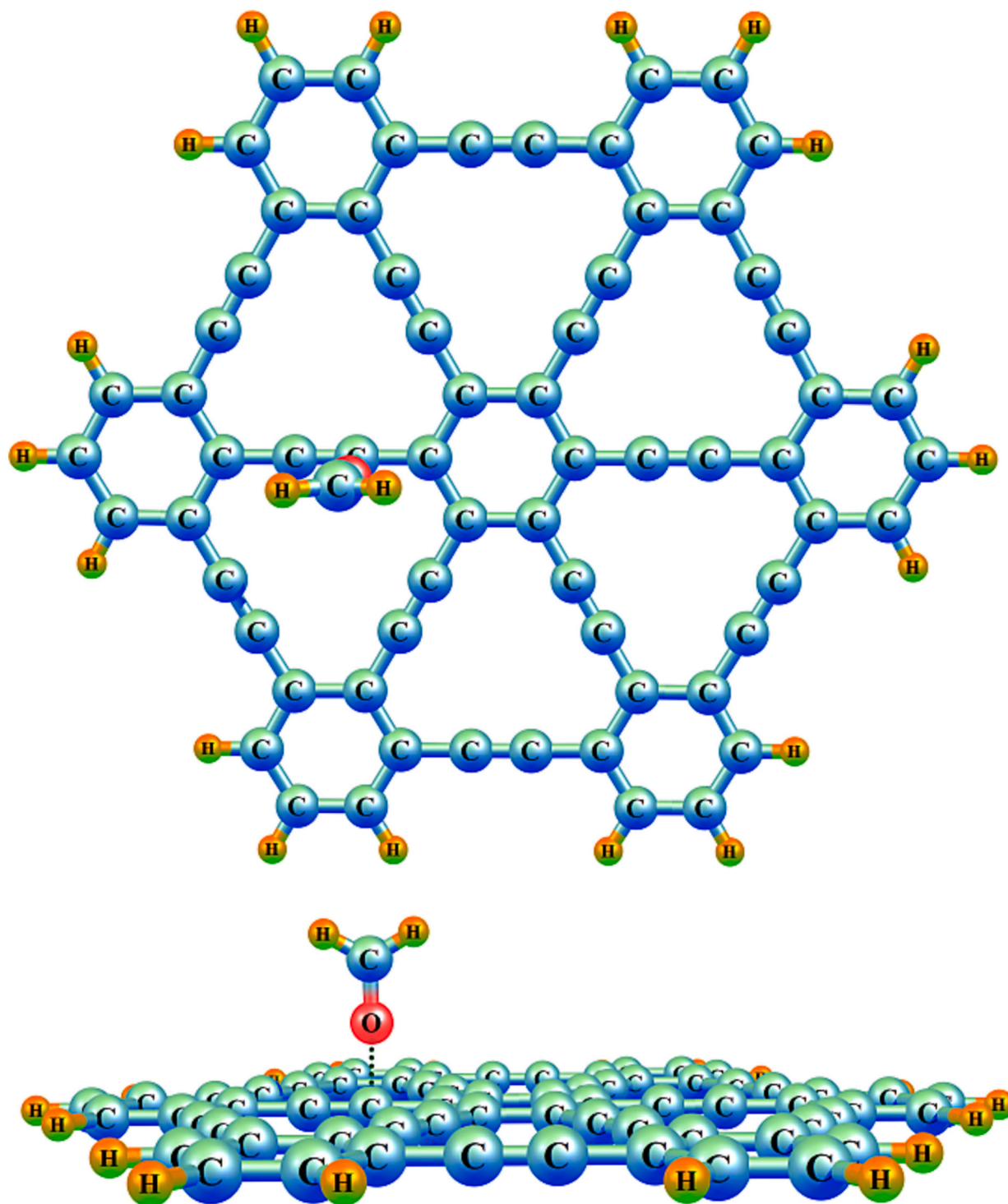


Fig. 5. The schematic of optimized structure for PGRD with CH_2O complex.

3.4. Electrostatic potential analysis (EPA)

Taking into account the electrostatic impacts throughout the process of adhesion is important to examine the intermolecular adhesion behavior. The computed electrostatic potential (EP) on the Pt@GRD can be seen in Fig. 7. The EP diagram is green in color at all sites in the changed GRD apart from the Pt atom, and it shows a negligible charge transport. The red or yellow color is the Pt atom, and it shows the likelihood of a reaction at this site [42]. After the adhesion of CH_2O onto the changed GRD, the C atoms surrounding the Pt atom donated

electrons to the region between CH_2O and the Pt atom for increasing the attractions between CH_2O and the surface and the O atom gained electrons throughout the adhesion process.

3.5. Analysis of inductive attributes and frontier molecular orbital (FMO) theory

One of the important parameters in monitoring gasses is the sensitivity of gas sensors. Safety hazards can be eliminated by using highly sensitive gas sensors. By carefully analyzing the adhesion energies,

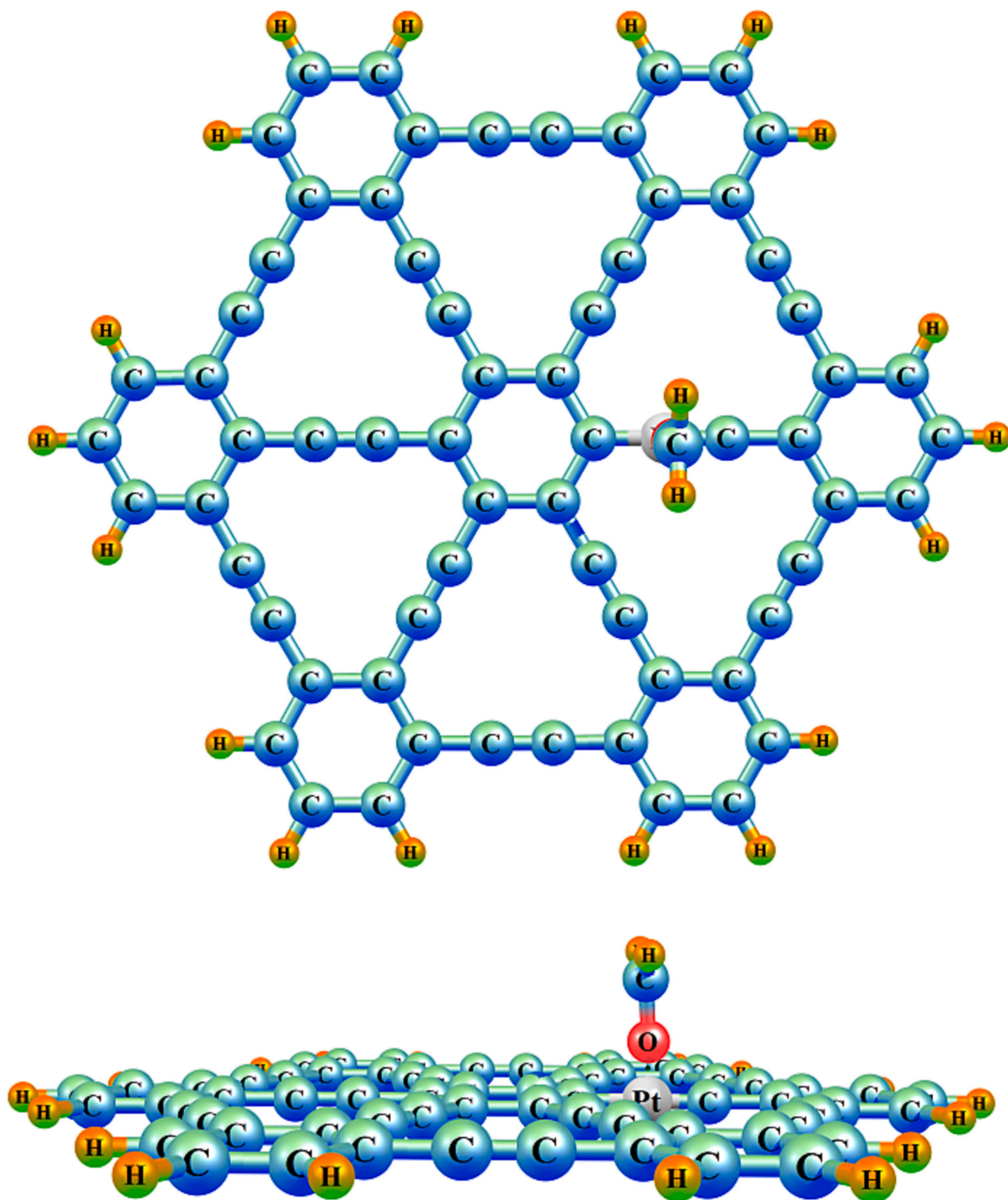


Fig. 6. The schematic of optimized structure for Pt@GRD with CH₂O complex.

Table 3
adhesion energies (E_{ads}), adhesion distance (D), and bandgap (E_g) of the CH₂O adhered onto the Pt@GRD.

Systems	E_{ads} (eV)	D (Å)	E_g (eV)
Pt@GRD	–	–	1.95
Pt@GRD/CH ₂ O	–1.57	1.83	1.19

adhesion distances, DOSs, and electrostatic potentials theoretically, we found that CH₂O had a stable adhesion on the Pt@GRD. The FMO theory was used for predicting the conductance of Pt@GRD theoretically to show the possibility of employing it as a novel 2D material in practical electrical installations since the bandgap of a 2D material and its sensitivity are related based on the equation below [61]:

$$S \propto \exp\left(\frac{|\Delta E_g|}{2kT}\right) \quad (8)$$

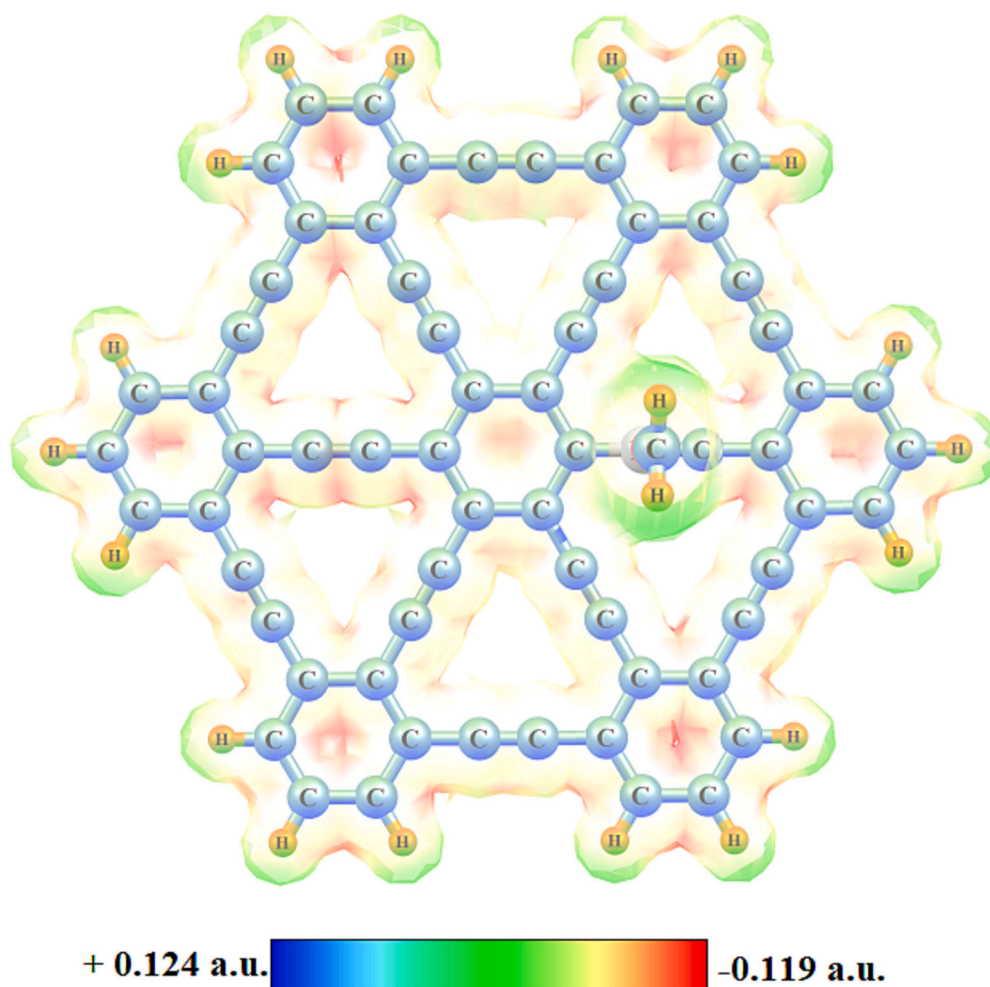


Fig. 7. The electrostatic potential of CH₂O adhesion onto Pt@GRD.

where ΔE_g , K and T , respectively, are the difference in bandgap prior to and following the adhesion, the temperature, and the Boltzmann constant ($8.62 \times 10^{-5} \text{ eV K}^{-1}$). Hence, the ΔE_g value can be used to assess the sensitivity of the CH₂O adhesion system.

As shown in Fig. 8 and Table 4, there was a decrease in the bandgap of the CH₂O adhesion system, which demonstrated a strong chemical adhesion of CH₂O molecules on the P@GRD and the viable use of Pt@GRD as an appropriate sensing material for CH₂O. There was no significant change in the HOMO distribution in the CH₂O adsorbed system in comparison with Pt@GRD, whereas there was a significant change in the HOMO distribution, which was line with the previously computed obtained bandgap values. In short, the chemical response of Pt@GRD towards CH₂O was good, which shows its potential as a sensing material.

Table 5 displays the quantum molecular descriptors of all the samples that were computed, showcasing their electronic properties and chemical reactivities. A material having smaller values of μ , η , and E_g generally indicates a higher level of chemical reactivity and simpler charge transport. Additionally, a molecule possessing a higher electrophilicity index (ω) is deemed to have superior electrophilic properties. The ionization potential (I) of a Pt@GRD can impact its hole injection ability. A reduced I typically suggests an improved hole injection capability. The Pt-doped GRD has the smallest I value of 3.56 eV compared to the undoped GRD. This suggests that the Pt-doped GRD might hold the greatest potential to be used in sensors due to its superior hole injection capability. The chemical stability of a material is often associated with its hardness (η), which is a measure of its resistance to

reactivity. Hence based on the η the tendency to interact with Pt@GRD with CH₂O is more than pristine GRD.

3.6. Recovery time

The time needed for gas desorption from the surface of a material is a crucial indicator in evaluating the sensing capability of sensor material and is referred to as recovery time. The recovery time can be calculated as follows:

$$\tau = A^{-1} \exp\left(\frac{-E_d}{kT}\right) \quad (9)$$

Herein, A is attempt frequency constant, which is 10^{12} s^{-1} [62]. Furthermore, the energy barrier that must be overcome during the desorption process is often substituted by the adsorption energy and the test temperature, represented by E_{ad} and T , respectively. At 298 K and 598 K, the desorption time of CH₂O in the Pt@GRD monolayer has been computed. At a temperature of 298 K, CH₂O release from Pt@GRD monolayer is basically inaccessible. Thus, it can be inferred that CH₂O gas is capable of maintaining a stable existence within Pt@GRD monolayer. However, it exhibits a relatively short desorption time on the material surface up to 598 K, averaging about 0.76 s.

4. Conclusion

The adhesion mechanism of CH₂O was carefully investigated on the PGRD and Pt@GRD through DFT calculations. Also, several properties of

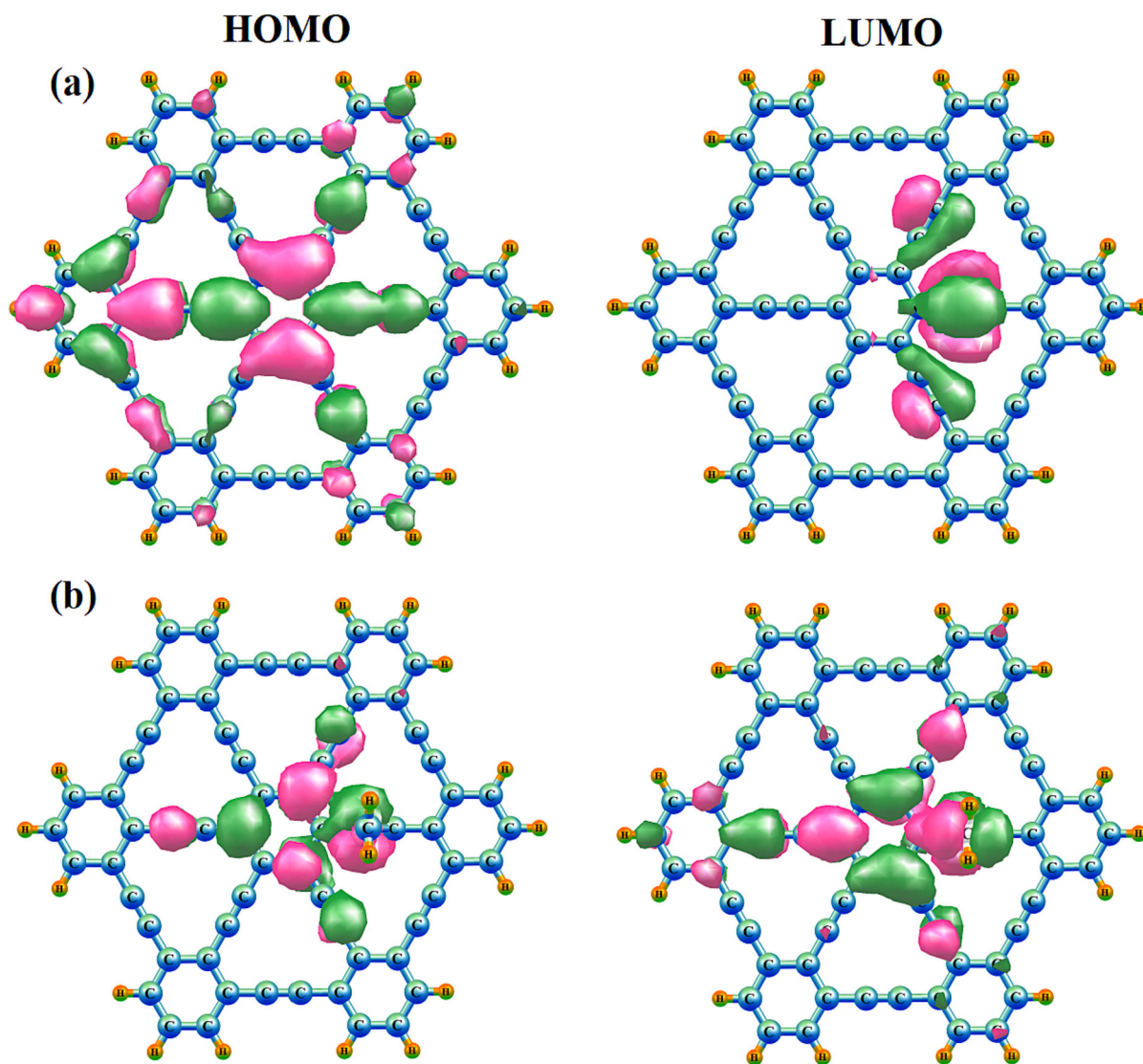


Fig. 8. The schematic of HOMO and LUMO distributions for (a) Pt@GRD (a) and (b) Pt@GRD/CH₂O.

Table 4

Computed parameters of the frontier orbitals in the system prior to and following the adhesion of by PGRD and Pt@GRD.

Systems	E_{HOMO} (eV)	E_{LUMO} (eV)	E_g (eV)
GRD	-4.90	-2.44	2.46
GRD-CH ₂ O	-4.80	-2.41	2.39
Pt@GRD	-3.56	-1.61	1.95
Pt@GRD/CH ₂ O	-2.78	-1.59	1.19

Table 5

The value of quantum molecular descriptors for PGRD and Pt@GRD.

Systems	I (eV)	A (eV)	μ (eV)	χ (eV)	η (eV)	ω (eV)
GRD	4.90	2.44	-3.67	3.67	1.23	5.48
GRD-CH ₂ O	4.80	2.41	-3.61	3.61	1.20	5.44
Pt@GRD	3.56	1.61	-2.59	2.59	0.98	3.43
Pt@GRD/CH ₂ O	2.78	1.59	-2.19	2.19	0.60	4.01

CH₂O such as the HOMO/LUMO energy level difference, electrostatic potential, density of states and adhesion energy were investigated. Based on the results, CII was the most suitable site for doping the Pt atom on the acetylene chain, which was the most stable CFG with the smallest

BE. Furthermore, doping the Pt atom decreased the bandgap from 2.46 eV to 1.95 eV in the PGRD, and there was an enhancement in the conductance and electrochemical reaction attributes. Additionally, CH₂O did not have a satisfactory adhesion on the PGRD, but Pt@GRD dramatically improved the chemical adhesion, which was due to the overlapping between the molecular orbitals of CH₂O and the Pt-d orbitals. This allowed the occurrence of chemical reactions and hybridization between the orbitals, which was conducive to forming new bonds and the stable occurrence of the adhesion. So, Pt@GRD can be considered an appropriate 2D sensing material for CH₂O. Based on the HOMO/LUMO of the adhesion system, Pt@GRD was capable of changing conductance, rearranging charges and inducing hybridization effects during the adhesion of CH₂O. Hence, Pt@GRD is capable of monitoring CH₂O with adequate sensitivity, and it could be considered a suitable sensing material for gasses. The current study can provide a theoretical basis for designing 2D materials such as GDY for sensing toxic gasses.

CRediT authorship contribution statement

M.J Saadh, H. Kh. Mohammed, Ameer. A. J: Conceptualization, Methodology, Software, Writing, Conceptualization, Methodology; Sh. K. Saraswat, S. M. Mohealdeen, Sailawi. H. A: Methodology, Software, Writing - review & editing; M. Mudhafar, F.A. Dawood, Y.

Elmasry: Writing - original draft, Methodology, Software, review & editing, Management and responsibility for the research activity planning and execution.

Funding

None.

Ethical approval

Not required.

Declaration of competing interest

The authors declare that they have no known competing financial interests or personal relationships that could have appeared to influence the work reported in this paper.

Data availability

No data was used for the research described in the article.

Acknowledgments

The authors extend their appreciation to the Deanship of Scientific Research at King Khalid University for funding this work through the Large Groups under grant number (RGP.2/582/44).

References

- Z. Wang, Z. Huang, J. Yu, X. Shao, W. Peng, J. Yu, Y. Jiang, Growth of Ag/g-C₃N₄ nanocomposites on nickel foam to enhance photocatalytic degradation of formaldehyde under visible light, *J. Environ. Sci.* 137 (2024) 432–442.
- M.B. Henda, S.H. Sadon, Z. Li, Q.H. Le, Removal of formaldehyde pollutant from petroleum industry wastewaters by polymers: a molecular dynamics simulation, *Eng. Anal. Bound. Elem.* 151 (2023) 400–405.
- H.Y. Ammar, CH₂O adsorption on M (M = Li, Mg and Al) atom deposited ZnO nano-cage: DFT study, *Key Eng. Mater.* 786 (2018) 384–392.
- H. Ammar, K.M. Eid, H. Badran, Interaction and detection of formaldehyde on pristine and doped boron nitride nano-cage: DFT calculations, *Mater. Today Commun.* 25 (2020), 101408.
- M. Li, Q. Guo, L. Chen, L. Li, H. Hou, Y. Zhao, Microstructure and properties of graphene nanoplatelets reinforced AZ91D matrix composites prepared by electromagnetic stirring casting, *J. Mater. Res. Technol.* 21 (2022) 4138–4150.
- T. Salthammer, Formaldehyde in the ambient atmosphere: from an indoor pollutant to an outdoor pollutant? *Angew. Chem. Int. Ed.* 52 (2013) 3320–3327.
- L. Zhu, D.J. Jacob, F.N. Keutsch, L.J. Mickley, R. Scheffe, M. Strum, G. González Abad, K. Chance, K. Yang, B. Rappenglück, Formaldehyde (HCHO) as a hazardous air pollutant: mapping surface air concentrations from satellite and inferring cancer risks in the United States, *Environ. Sci. Technol.* 51 (2017) 5650–5657.
- D. Cockcroft, V. Hoepfner, J. Dolovitch, Occupational asthma caused by cedar urea formaldehyde particle board, *Chest* 82 (1982) 49–53.
- J. Ye, X. Zhu, B. Cheng, J. Yu, C. Jiang, Few-layered graphene-like boron nitride: a highly efficient adsorbent for indoor formaldehyde removal, *Environ. Sci. Technol. Lett.* 4 (2017) 20–25.
- V.J. Cogliano, Y. Grosse, R.A. Baan, K. Straif, M.B. Secretan, F.E. Ghisssassi, W.G.f. V., 88, Meeting report: summary of IARC monographs on formaldehyde, 2-butoxyethanol, and 1-tert-butoxy-2-propanol, *Environ. Health Perspect.* 113 (2005) 1205–1208.
- L. Zhang, C. Steinmaus, D.A. Eastmond, X.K. Xin, M.T. Smith, Formaldehyde exposure and leukemia: a new meta-analysis and potential mechanisms, *Mutat. Res. Rev. Mutat. Res.* 681 (2009) 150–168.
- S.M. Wang, X.T. Mu, H.R. Liu, S.T. Zheng, Q.Y. Yang, Pore-structure control in metal-organic frameworks (MOFs) for capture of the greenhouse gas SF₆ with record separation, *Angew. Chem.* 134 (2022), e202207066.
- T. Hasell, M. Miklitz, A. Stephenson, M.A. Little, S.Y. Chong, R. Clowes, L. Chen, D. Holden, G.A. Tribello, K.E. Jelfs, Porous organic cages for sulfur hexafluoride separation, *J. Am. Chem. Soc.* 138 (2016) 1653–1659.
- I.A. Riddell, M.M. Smulders, J.K. Clegg, J.R. Nitschke, Encapsulation, storage and controlled release of sulfur hexafluoride from a metal-organic capsule, *Chem. Commun.* 47 (2011) 457–459.
- X. Zhang, L. Yu, Y. Gui, W. Hu, First-principles study of SF₆ decomposed gas adsorbed on Au-decorated graphene, *Appl. Surf. Sci.* 367 (2016) 259–269.
- D. Chen, X. Zhang, J. Tang, H. Cui, Y. Li, G. Zhang, J. Yang, Density functional theory study of small Ag cluster adsorbed on graphyne, *Appl. Surf. Sci.* 465 (2019) 93–102.
- K.S. Novoselov, A.K. Geim, S.V. Morozov, D. Jiang, M.I. Katsnelson, I. V. Grigorieva, S. Dubonos, A.A. Firsov, Two-dimensional gas of massless Dirac fermions in graphene, *Nature* 438 (2005) 197–200.
- Q. Zhou, W. Chen, L. Xu, R. Kumar, Y. Gui, Z. Zhao, C. Tang, S. Zhu, Highly sensitive carbon monoxide (CO) gas sensors based on Ni and Zn doped SnO₂ nanomaterials, *Ceram. Int.* 44 (2018) 4392–4399.
- P. Ren, L. Qi, K. You, Q. Shi, Hydrothermal synthesis of hierarchical SnO₂ nanostructures for improved formaldehyde gas sensing, *Nanomaterials* 12 (2022) 228.
- S. Dong, H. Zhang, D. Yuan, Supramolecular nonwoven materials via thermally induced precursor crystallization of nanocrystalline fibers/belts for recyclable air filters, *ACS Appl. Nano Mater.* 6 (2023) 9548–9557.
- W. Kuang, H. Wang, X. Li, J. Zhang, Q. Zhou, Y. Zhao, Application of the thermodynamic extremal principle to diffusion-controlled phase transformations in Fe-CX alloys: modeling and applications, *Acta Mater.* 159 (2018) 16–30.
- S. Hou, R. Pang, S. Chang, L. Ye, J. Xu, X. Wang, Y. Zhang, Y. Shang, A. Cao, Synergistic CNFs/CoS₂/MoS₂ flexible films with unprecedented selectivity for NO gas at room temperature, *ACS Appl. Mater. Interfaces* 12 (2020) 29778–29786.
- I. Choudhuri, D. Sadhukhan, P. Garg, A. Mahata, B. Pathak, Lewis acid–base adducts for improving the selectivity and sensitivity of graphene based gas sensors, *ACS Sensors* 1 (2016) 451–459.
- M. Shukri, M. Saimin, M. Yaakob, M. Yahya, M. Taib, Structural and electronic properties of CO and NO gas molecules on Pd-doped vacancy graphene: a first principles study, *Appl. Surf. Sci.* 494 (2019) 817–828.
- Y. Tang, Z. Liu, Z. Shen, W. Chen, D. Ma, X. Dai, Adsorption sensitivity of metal atom decorated bilayer graphene toward toxic gas molecules (CO, NO, SO₂ and HCN), *Sens. Actuators B* 238 (2017) 182–195.
- W. Zhao, H. Suo, S. Wang, L. Ma, L. Wang, Q. Wang, Z. Zhang, Mg gas infiltration for the fabrication of MgB₂ pellets using nanosized and micro-sized B powders, *J. Eur. Ceram. Soc.* 42 (2022) 7036–7048.
- T. Tang, M. Zhou, J. Lv, H. Cheng, H. Wang, D. Qin, G. Hu, X. Liu, Sensitive and selective electrochemical determination of uric acid in urine based on ultrasmall iron oxide nanoparticles decorated urchin-like nitrogen-doped carbon, *Colloids Surf. B Biointerfaces* 216 (2022), 112538.
- X. Zhou, M. You, F. Wang, Z. Wang, X. Gao, C. Jing, J. Liu, M. Guo, J. Li, A. Luo, Multifunctional graphdiyne–cerium oxide nanozymes facilitate microRNA delivery and attenuate tumor hypoxia for highly efficient radiotherapy of esophageal cancer, *Adv. Mater.* 33 (2021) 2100556.
- J. Liu, L. Wang, X. Shen, X. Gao, Y. Chen, H. Liu, Y. Liu, D. Yin, Y. Liu, W. Xu, Graphdiyne-templated palladium-nanoparticle assembly as a robust oxygen generator to attenuate tumor hypoxia, *Nano Today* 34 (2020), 100907.
- P. Kuang, M. He, H. Zou, J. Yu, K. Fan, OD/3D MoS₂-NIS₂/N-doped graphene foam composite for efficient overall water splitting, *Appl. Catal. Environ.* 254 (2019) 15–25.
- Z. Jin, Q. Zhou, Y. Chen, P. Mao, H. Li, H. Liu, J. Wang, Y. Li, Graphdiyne: ZnO nanocomposites for high-performance UV photodetectors, *Adv. Mater.* 28 (2016) 3697–3702.
- Y. Xue, J. Li, Z. Xue, Y. Li, H. Liu, D. Li, W. Yang, Y. Li, Extraordinarily durable graphdiyne-supported electrocatalyst with high activity for hydrogen production at all values of pH, *ACS Appl. Mater. Interfaces* 8 (2016) 31083–31091.
- Q. Xu, B. Zhu, B. Cheng, J. Yu, M. Zhou, W. Ho, Photocatalytic H₂ evolution on graphdiyne/g-C₃N₄ hybrid nanocomposites, *Appl. Catal. Environ.* 255 (2019), 117770.
- P. Kuang, B. Zhu, Y. Li, H. Liu, J. Yu, K. Fan, Graphdiyne: a superior carbon additive to boost the activity of water oxidation catalysts, *Nanoscale Horizons* 3 (2018) 317–326.
- L. Zhang, D. Qin, J. Feng, T. Tang, H. Cheng, Rapid quantitative detection of luteolin using an electrochemical sensor based on electrospinning of carbon nanofibers doped with single-walled carbon nanoangles, *Anal. Methods* 15 (2023) 3073–3083.
- H. Wang, T. Yang, J. Wu, D. Chen, W. Wang, Unveiling the mystery of SUMO-activating enzyme subunit 1: a groundbreaking biomarker in the early detection and advancement of hepatocellular carcinoma, in: *Transplantation Proceedings*, Elsevier, 2023, pp. 945–951.
- Y. Li, L. Xu, H. Liu, Y. Li, Graphdiyne and graphyne: from theoretical predictions to practical construction, *Chem. Soc. Rev.* 43 (2014) 2572–2586.
- S. Kim, J.Y. Lee, Doping and vacancy effects of graphyne on SO₂ adsorption, *J. Colloid Interface Sci.* 493 (2017) 123–129.
- Z. Lu, P. Lv, D. Ma, X. Yang, S. Li, Z. Yang, Detection of gas molecules on single Mn adatom adsorbed graphyne: a DFT-D study, *J. Phys. D Appl. Phys.* 51 (2018), 065109.
- X. Zhang, R. Fang, D. Chen, G. Zhang, Using Pd-doped γ -graphyne to detect dissolved gases in transformer oil: a density functional theory investigation, *Nanomaterials* 9 (2019) 1490.
- T. Hussain, M. Sajjad, D. Singh, H. Bae, H. Lee, J.A. Larsson, R. Ahuja, A. Karton, Sensing of volatile organic compounds on two-dimensional nitrogenated holey graphene, graphdiyne, and their heterostructure, *Carbon* 163 (2020) 213–223.
- Y. Zhao, J. Wan, H. Yao, L. Zhang, K. Lin, L. Wang, N. Yang, D. Liu, L. Song, J. Zhu, Few-layer graphdiyne doped with sp-hybridized nitrogen atoms at acetylenic sites for oxygen reduction electrocatalysis, *Nat. Chem.* 10 (2018) 924–931.
- M. Dehkhodaei, A. Reisi-Vanani, Effect of the charge injection and N and S co-doping on the structural and electronic properties, and hydrogen storage capacity of graphdiyne 2D structure, *Surf. Interfaces* 31 (2022), 102031.
- Y. Liu, T. Shi, Q. Si, T. Liu, Adsorption and sensing performances of transition metal (Pd, Pt, Ag and Au) doped MoTe₂ monolayer upon NO₂: a DFT study, *Phys. Lett. A* 391 (2021), 127117.

- [45] M.W. Schmidt, K.K. Baldrige, J.A. Boatz, S.T. Elbert, M.S. Gordon, J.H. Jensen, S. Koseki, N. Matsunaga, K.A. Nguyen, S. Su, T.L. Windus, M. Dupuis, J. A. Montgomery Jr., General atomic and molecular electronic structure system, *J. Comput. Chem.* 14 (1993) 1347–1363.
- [46] S. Grimme, Accurate description of van der Waals complexes by density functional theory including empirical corrections, *J. Comput. Chem.* 25 (2004) 1463–1473.
- [47] J. Beheshtian, A.A. Peyghan, Z. Bagheri, Detection of phosgene by Sc-doped BN nanotubes: a DFT study, *Sens. Actuators B* 171 (2012) 846–852.
- [48] J. Beheshtian, A.A. Peyghan, M.B. Tabar, Z. Bagheri, DFT study on the functionalization of a BN nanotube with sulfamide, *Appl. Surf. Sci.* 266 (2013) 182–187.
- [49] H. Tachikawa, Hydrogen atom addition to the surface of graphene nanoflakes: a density functional theory study, *Appl. Surf. Sci.* 396 (2017) 1335–1342.
- [50] L. Chen, Y. Zhao, M. Li, L. Li, L. Hou, H. Hou, Reinforced AZ91D magnesium alloy with thixomolding process facilitated dispersion of graphene nanoplatelets and enhanced interfacial interactions, *Mater. Sci. Eng. A* 804 (2021), 140793.
- [51] P. Wu, Y. Li, S. Xiao, J. Chen, J. Tang, D. Chen, X. Zhang, SnO₂ nanoparticles based highly sensitive gas sensor for detection of C₄F₇N: a new eco-friendly gas insulating medium, *J. Hazard. Mater.* 422 (2022), 126882.
- [52] Q. Sun, Z. Li, D.J. Searles, Y. Chen, G. Lu, A. Du, Charge-controlled switchable CO₂ capture on boron nitride nanomaterials, *J. Am. Chem. Soc.* 135 (2013) 8246–8253.
- [53] L. Zhu, Q. Xue, X. Li, T. Wu, Y. Jin, W. Xing, C₂N: an excellent two-dimensional monolayer membrane for He separation, *J. Mater. Chem. A* 3 (2015) 21351–21356.
- [54] V. Zaverkin, J. Kästner, Gaussian moments as physically inspired molecular descriptors for accurate and scalable machine learning potentials, *J. Chem. Theory Comput.* 16 (2020) 5410–5421.
- [55] P. Singla, M. Riyaz, S. Singhal, N. Goel, Theoretical study of adsorption of amino acids on graphene and BN sheet in gas and aqueous phase with empirical DFT dispersion correction, *Phys. Chem. Chem. Phys.* 18 (2016) 5597–5604.
- [56] J. Tomasi, M. Persico, Molecular interactions in solution: an overview of methods based on continuous distributions of the solvent, *Chem. Rev.* 94 (1994) 2027–2094.
- [57] J. Kim, S. Kang, J. Lim, W.Y. Kim, Study of Li adsorption on graphdiyne using hybrid DFT calculations, *ACS Appl. Mater. Interfaces* 11 (2018) 2677–2683.
- [58] D. Chen, X. Zhang, J. Tang, Z. Cui, H. Cui, Pristine and Cu decorated hexagonal InN monolayer, a promising candidate to detect and scavenge SF₆ decompositions based on first-principle study, *J. Hazard. Mater.* 363 (2019) 346–357.
- [59] Z. Li, L. Jia, J. Chen, X. Cui, W. Zeng, Q. Zhou, Ag-modified hexagonal GaN monolayer as an innovative gas detector toward SF₆ decomposed species: insights from the first-principles computations, *Appl. Surf. Sci.* 589 (2022), 153000.
- [60] J. Wu, J. Zhang, Z. Cao, Q. Liu, F. Wei, J. Zhou, D. Wang, S. Shi, G. Qian, Improvement on fluorine migration from SF₆ to SiF₄ by an efficient mediator of Fe₂O₃/Cr₂O₃ composites, *ACS Appl. Mater. Interfaces* 11 (2019) 16538–16545.
- [61] Y. Wang, T. Li, Y. Peng, Y. Gui, H. Sun, Pd and Pt decorated GeSe monolayers as promising materials for SOF₂ and SO₂F₂ sensing, *Appl. Surf. Sci.* 560 (2021), 150028.
- [62] J. Min Lee, S. Ho Lim, Thermally activated magnetization switching in a nanostructured synthetic ferrimagnet, *J. Appl. Phys.* 113 (2013), 063914.